

Jet Energy Reconstruction in the ATLAS Barrel Calorimeters Using Combined Beam Test Data

T. Davídek

Institute of Particle and Nuclear Physics,
Charles University, Prague

ATL-TILECAL-2000-010

11/05/2000



Abstract

The method of the parton energy reconstruction in the barrel part of the ATLAS calorimeter system (electromagnetic LAr and hadronic Tile calorimeter) is presented. The results are based on the experimental data obtained during the combined LAr+Tilecal beam test in April 1996 – particles of gluon and light quark jets generated by Pythia and Jetset are replaced by the electron and hadron events. The applied method recovers the linearity within $\pm 0.5\%$ up to 1 TeV and improves the energy resolution. The implications for the LVL1 trigger are discussed as well.

1 Introduction

The main task of the calorimetry system is to measure the energy and direction of the incoming jets. The important characteristics are the linearity and resolution of the measured energy.

The presented analysis is based on the calorimeter data obtained during the combined LAr+Tilecal beam test carried out in the SPS H8 beam line in 1996. Although the calorimeter prototypes used in the beam test [1, 2] differ from the final ATLAS design (see Fig. 1), the same main structure (total length of the LAr calorimeter, amount of the dead material between the LAr and Tile calorimeters) allows us to construct the ATLAS calorimeter response to jets using these beam test data.

2 Calorimeter Signal

In order to emulate the ATLAS calorimeter response to jets, the following procedure has been accommodated: first, jet particles are produced using Pythia and Jetset MC generator [3]. Then all the particles are tracked in the solenoid magnetic field, which corresponds to that in the ATLAS detector (field strength

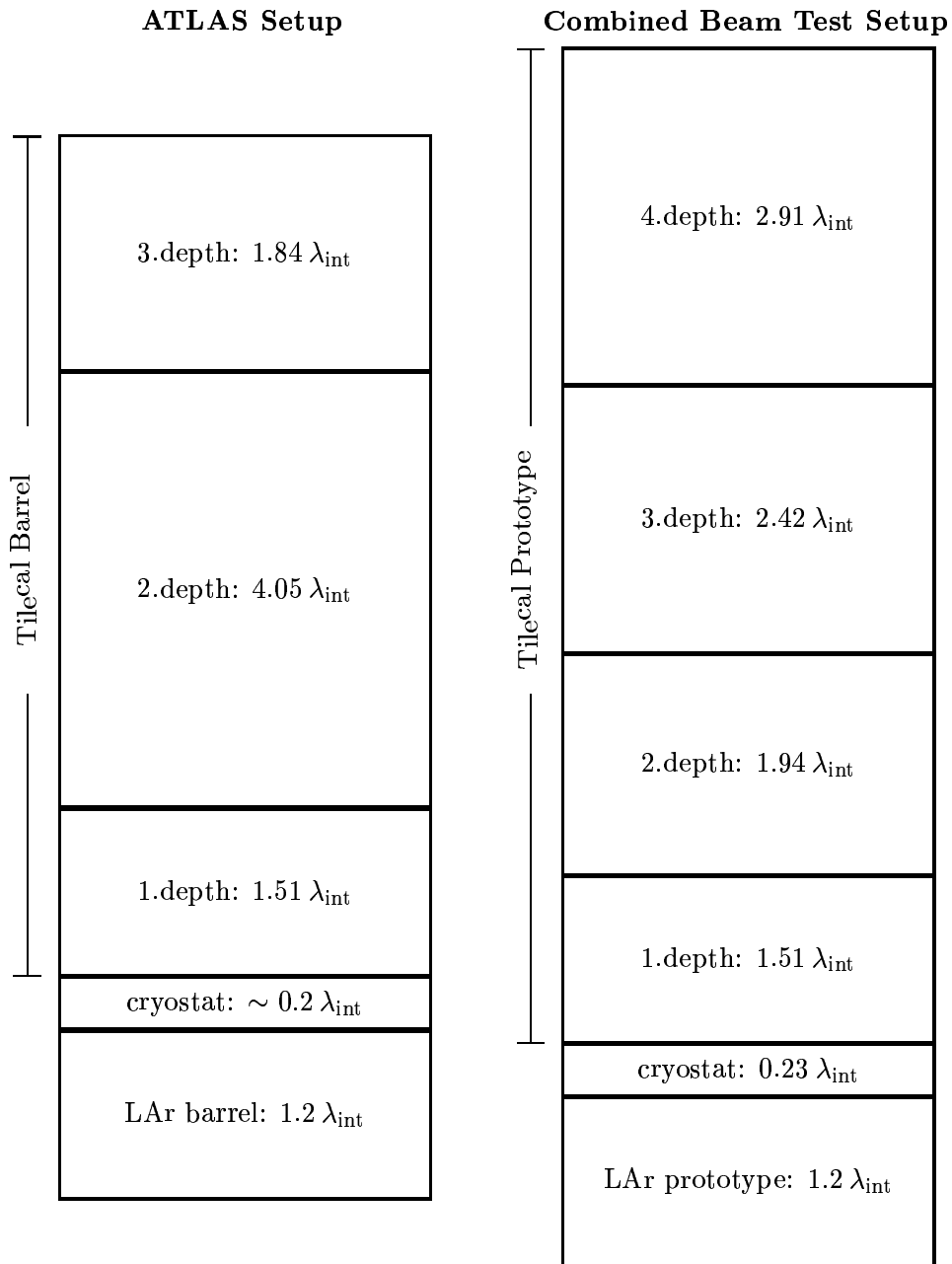


Figure 1: Although the radial segmentation of both LAr and Tilecal prototypes differ from that of the real ATLAS setup, the total length of the electromagnetic LAr calorimeter and dead material between the two calorimeters are the same.

$B = 2$ T, radius $R = 1.15$ m). Finally, all the particles are substituted by the corresponding events from the beam test data and the response in all calorimeter samplings is constructed.

2.1 Data Selection

During the mentioned beam test period, particles entered the LAr prototype at the fixed angle 12 deg, which corresponds to ATLAS $\eta = 0.2$. Data sets of positrons/electrons (20, 40, 50, 80, 100, 150, 180 and 287.5 GeV) and hadrons (10, 20, 40, 50, 80, 100, 150, 180 and 300 GeV) were obtained in this beam test. The basic scheme of the experimental setup is shown in Fig. 2, the detailed description can be found in Refs. [1, 2].

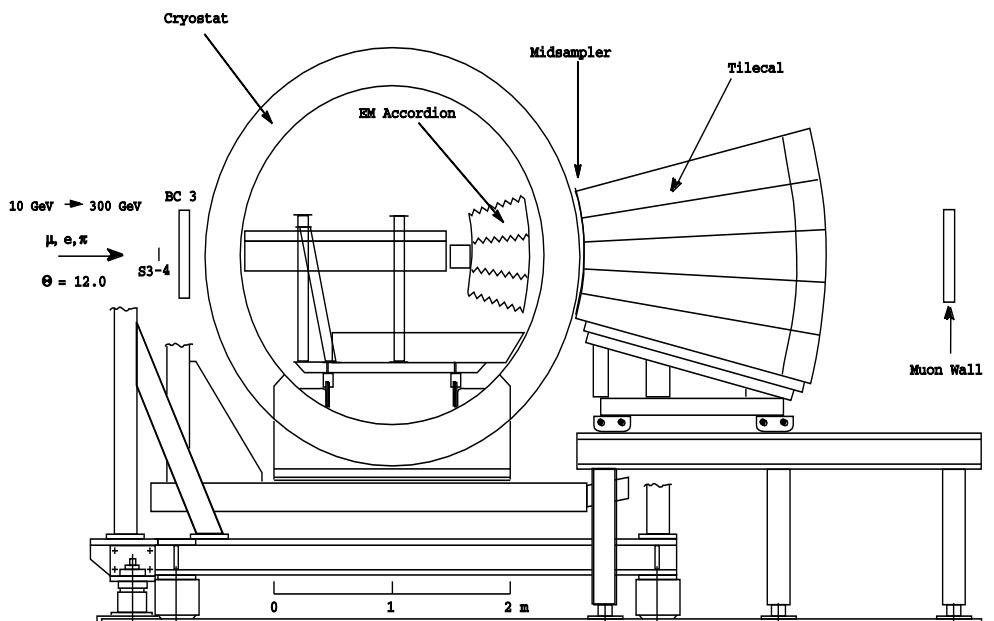


Figure 2: The combined beam test setup in April 1996.

A set of common cuts is used for all particle types. Their nature is the following (see Ref. [1] for more details):

- Events with tracks either not parallel with the beam direction (i.e. at angles > 1.5 mrad with respect to the beam axis) or parallel but far (> 2 cm) from the beam centre are removed. Data from beam chambers are used for this purpose. These cuts remove beam halo particles and improves the beam momentum width.
- Events with beam scintillator signal incompatible with that of a minimum ionizing particle (mip) are discarded to avoid the case when either 2 particles enter the calorimeter within the same trigger or the interaction started upstream.

- Events starting the shower upstream in the cryostat are removed. This is done using the presampler signal and impact position reconstructed by beam chambers and presampler. Their difference results in a Gaussian distribution with large tails on both sides. These tails are either due to particle interaction in front of the presampler or because of the noise. Only events with the impact point difference within $\pm 3\sigma$ of the Gaussian core are kept for further analysis.

Additional cuts are applied in order to select the respective particle type:

2.1.1 Additional Cuts for Muons

Muons are extracted from the hadron data by imposing the total energy cut. Moreover, since muons pass through the calorimeter system, they are detected both in Midsamplers and in the back muon wall counters. Therefore, three additional cuts are applied to pick up muon events from hadron beams:

- The total energy (LAr+Tilecal) is low (e.g. less than 8 GeV for 20 GeV beam).
- In the Midsampler, the central counters (i.e. those pointed to by the beam) give a signal compatible with a single particle passage. No signal in the remaining Midsampler counters is required.
- The back muon wall counters pointed to by the beam are hit.

2.1.2 Pion/Proton Separation

The hadron beams were of positive charge (except of the highest energy), therefore they consist of pions, kaons and protons. Whereas the kaon fraction is very small (less than 5%), the proton fraction increases with the beam energy, being approximately 1:1 with respect to pions at 80 GeV (see e.g. Ref. [4]).

Due to the different masses (which implies different velocity β at the same beam momentum), pions and protons can in principle be distinguished with the Cerenkov detector. The Cerenkov threshold counter installed in H8 beam line enabled the pion/proton separation for 40, 50 and 80 GeV beams.

2.1.3 Cuts for Positrons

Possible pion admixture in the electron/positron beams would affect in particular the last Tilecal sampling response. Therefore, in addition to the common cuts mentioned above, special cuts are applied here to remove pion events. The electromagnetic and hadronic showers differ in the size, so these cuts are based both on the radial and longitudinal shower size in the fine-segmented LAr calorimeter. Finally, a cross-check is done using the Cerenkov counter – all the electron/positron events must emit Cerenkov photons.

2.2 Calorimeter Calibration

Both calorimeters are calibrated to the electromagnetic scale. The energy scale in the LAr prototype is set up with 100 GeV electrons, which in the signal window used for pion energy reconstruction¹ results in the multiplicative coefficient $c_{\text{LAr}} = 1.1$ (see also Ref. [1, 2]).

In Tilecal prototypes, the signal of 100 GeV pions is exploited to set up the energy scale. This is done with pion events starting the shower in Tilecal, i.e. their response in the electromagnetic part and in the Midsampler is compatible with that of a minimum ionizing particle. Taking into account $e/h = 1.30$ [5] in Tilecal and the e/π ratio energy dependence

$$\left(\frac{e}{\pi}\right) = \frac{e/h}{1 + (e/h - 1) \times 0.11 \times \ln E} \quad (1)$$

the charge-to-energy conversion coefficient amounts to $c_{\text{Tile}} = 0.146$ GeV/pC.

2.3 Particles Substitution

In order to construct the real calorimeter signal, all particles coming from the Pythia and Jetset MC generator are replaced by the corresponding events from the available beam test data sets.

The elmg. particles (i.e. those producing pure electromagnetic cascades in the calorimeter) — electron, positron and photon — are replaced by the respective electron/positron event, muons are substituted by a muon event. The substitution of hadrons is the following:

- Hadrons with a short life-time (K_S^0 , Λ^0 and heavier baryons) are “forced to decay” before entering the calorimeter, i.e. they are substituted by their decay products at respective energies. K_S^0 always decays to 2 pions and heavy baryons are replaced as they would have decayed to proton and pion. Such unstable hadrons represent only less than 1% of all particles.
- Other hadrons are replaced by appropriate pion events, except of those in the energy range 40 to 80 GeV, where the pion/proton separation is exploited:
 - Baryons (protons and neutrons) are substituted by a corresponding proton event.
 - Mesons are replaced by pion events.

The beam test data are available at various but discrete energies. The energy of the beam particle (denoted E_{beam}) replacing the generated one (energy E_{gen}) is chosen in the following way:

- If $E_{\text{gen}} > E_{\text{beam}}^{\text{min}}$ (the lowest available beam energy of the respective beam particle) then the closest upper or lower beam energy to E_{gen} is taken so that the mean energies $\langle E_{\text{beam}} \rangle$ and $\langle E_{\text{gen}} \rangle$ of all particles of the given type (e^- , e^+ , π^+ , π^- , K^- etc.) are the same.

¹The size of the signal window used in the LAr calorimeter depends on the particle type – see Section 2.4.

- Elmg. particles and hadrons with the energy $E_{\text{gen}} < E_{\text{beam}}^{\text{min}}$ are summed in the so-called “low-energy jets”, grouping together particles closest in space. The respective number of low-energy jets (elmg. particles and hadrons are treated separately) is given by the formula

$$N(\text{low-E jet}) = \left[\frac{\sum E_{\text{gen}}}{E_{\text{beam}}^{\text{min}}} \right] + 1 \quad (2)$$

and each “low-energy jet” obeys the relation

$$E(\text{low-E jet}) \leq E_{\text{beam}}^{\text{min}} \quad (3)$$

Each such jet is then replaced by the respective beam particle at the energy $E_{\text{beam}}^{\text{min}}$.

- Muons with incident energies $E_{\text{gen}} < E_{\text{beam}}^{\text{min}}$ are always substituted by muon events at the minimal beam energy available.

2.4 Signal Construction

The jet direction $(\eta_{\text{jet}}, \varphi_{\text{jet}})$ is reconstructed with the standard cone algorithm available in Pythia. After that, the calorimeter signal is built up in the cone $R = 0.4$ around the jet axis.

The radial size of the second and third Tilecal prototype sampling roughly correspond to that of the second sampling of the real Tilecal barrel (see also Fig. 1). Moreover, the first sampling is of the same size both in the beam test and ATLAS design. Therefore, the two Tilecal prototype samplings (2,3) are summed up to emulate the adequate second sampling response in the ATLAS setup.

Thus, the calorimeter response to jets is constructed separately in each of the six calorimeter radial samplings – 3 in the LAr and 3 in Tile calorimeter. The procedure is the following:

- For each particle involved in the given jet event, its coordinates $\eta_{\text{part}}, \varphi_{\text{part}}$ are evaluated using the projected impact point into the radial centre of the sampling.
- Real $\eta_{\text{cell}}, \varphi_{\text{cell}}$ coordinates are assigned to all cells in the given beam test calorimeter sampling:

$$\eta_{\text{cell}} = \eta_{\text{part}} + \Delta\eta_{\text{cell}}(\text{beam test}) \quad (4)$$

where $\Delta\eta_{\text{cell}}(\text{beam test})$ represents the respective distance of the prototype cell from the beam axis.²

- The response of all cells inside the cone

$$(\eta_{\text{cell}} - \eta_{\text{jet}})^2 + (\varphi_{\text{cell}} - \varphi_{\text{jet}})^2 \leq R^2 \quad (5)$$

is summed up. However, additional restrictions are imposed in order to reduce the noise contribution:

²The formula (4) represents a simplified description. In fact all calculations are performed precisely using the x, y, z coordinates.

- Two different thresholds (either $3\sigma_{\text{noise}}$ or $1.5\sigma_{\text{noise}}$) are applied in each cell in the Tilecal prototypes. Lower signals are considered to be zero.
- In the LAr calorimeter prototype, the size of the read-out cell grid depends on the particle type (the same approach was applied in the combined data analysis, see Ref. [2]). Whereas 11×11 cells around the beam spot in the $\eta \times \varphi$ plane are considered for hadron events (pions or protons), electron/positron signal is read-out only from the 7×3 cells. The muon induced signal is sufficient to read-out from two neighbouring cells pointed to by the beam.
- Finally, the calorimeter response to the given particle is multiplied by the ratio $E_{\text{gen}}/E_{\text{beam}}$ in all samplings. This correction is applied to all particles but muons and accounts for the difference between the generated (coming from Pythia generator) and substituted particle's energy.

3 Reconstruction of the Parton Energy

The goal of the algorithm is to recover the energy of the incident parton, not only the energy of the jet particles entering the calorimeter. As the presented approach exploits only the calorimeter data, its simple modification can be used at the LVL1 trigger (see Section 4).

3.1 The Method

While in Tilecal the presented method exploits the e/h approach (applied to single hadron events – see Ref. [6]), the weighting function is used in the LAr calorimeter so that the original parton energy is recovered in the total. Under the assumption that the signal in Tilecal comes from hadronic showers only (i.e. the showers induced by incident electromagnetic particles are almost fully contained in the LAr part), the reconstructed energy reads

$$E_{\text{rec}} = \beta(E, R) \times \left(\alpha \times c_{\text{LAr}} \times S_{\text{LAr}} + \left(\frac{e}{\pi} \right)_{\text{Tile}} \times c_{\text{Tile}} \times S_{\text{Tile}} + E_{\text{cryo}} \right) \quad (6)$$

where S_{LAr} and S_{Tile} represent the signal in the LAr and Tile calorimeter respectively.

The cryostat represents the dead material between the two calorimeters (see Fig. 2). As shown in Ref. [1], the respective correction term E_{cryo} is proportional to the geometrical mean of the last LAr and the first Tilecal sampling:

$$E_{\text{cryo}} = c_{\text{cryo}} \times \sqrt{\alpha \times c_{\text{LAr}} \times S_{\text{LAr}}^{(3)} \times \left(\frac{e}{\pi} \right)_{\text{Tile}} \times c_{\text{Tile}} \times S_{\text{Tile}}^{(1)}} \quad (7)$$

The constant $c_{\text{cryo}} = 0.31$ is taken following the Ref. [6].

Taking into account the general formula (1), the $(e/\pi)_{\text{Tile}}$ parameter is evaluated in few iterative steps using the relation

$$\left(\frac{e}{\pi} \right)_{\text{Tile}} = \frac{(e/h)_{\text{Tile}}}{1 + ((e/h)_{\text{Tile}} - 1) \times 0.11 \times \ln((e/\pi)_{\text{Tile}} \times c_{\text{Tile}} \times S_{\text{Tile}})} \quad (8)$$

Usually, two steps are sufficient to achieve the accuracy better than 1%.

The function α plays the role of the weighted share of the electromagnetic and hadronic particles. It generally depends both on E_{LAr} and E_{Tile}

$$E_{\text{LAr}} = c_{\text{LAr}} \times S_{\text{LAr}} \quad (9a)$$

$$E_{\text{Tile}} = c_{\text{Tile}} \times S_{\text{Tile}} \quad (9b)$$

The best results (in terms of linearity and resolution) are achieved using the parametrization

$$\alpha = \alpha \left(\frac{E_{\text{LAr}}^{(1)} + E_{\text{LAr}}^{(2)}}{E_{\text{tot}}}, E_{\text{tot}} \right) \quad (10)$$

where $E_{\text{LAr}}^{(i)}$ denotes the energy deposited in the i -th radial sampling of the LAr calorimeter and the quantity E_{tot} is defined as

$$E_{\text{tot}} = E_{\text{LAr}} + \left(\frac{e}{\pi} \right)_{\text{Tile}} \times E_{\text{Tile}} + E_{\text{cryo}} \quad (\alpha = 1) \quad (11)$$

At the given E_{tot} , the α function can be parametrized by the formula

$$\alpha(x) \Big|_{E_{\text{tot}}=\text{const}} = A(1-x) + B(1-x)^2 + C(1-x)^3 + D \quad (12a)$$

$$x = \frac{E_{\text{LAr}}^{(1)} + E_{\text{LAr}}^{(2)}}{E_{\text{tot}}} \quad (12b)$$

The case $x = 1$ corresponds to the situation, when all the energy is absorbed in the LAr calorimeter. As also some hadrons can be contained in such jet event, $D > 1$ (due to the non-compensation $-(e/h)_{\text{LAr}} > 1$). The fit (12a) applied to the α function is shown in Fig. 3 (left plot).

The α dependence on the second variable E_{tot} is described by introducing the A, B, C, D to be the functions of the quantity E_{tot} . It turns out that all these parameters decrease with this energy variable and their dependence can be described as a sum of two exponentials (see the right plot in Fig. 3).

The function $\beta(E, R)$ in the formula (6) accounts for the part of the jet energy not detected in the calorimeter. There are several effects, which this function corrects for:

- A part of the jet energy is represented by the very low- p_{T} ($p_{\text{T}} < 0.5$ GeV) charged particles, which are caught in the solenoid magnetic field, thus they do not enter the calorimeter. As this effect dominates for the low jet energies, β decreases with the increasing jet energy.
- The jet energy is read-out from the cone of a certain size R . The energy outside such cone is not taken into account.
- Some part of energy may escape out of the calorimeter due to muons or non-interacting neutrinos.

The β function is obtained as the ratio of the original parton's energy and of the total energy of all particles (except muons and neutrinos) entering the calorimeter. The β dependence on the original gluon energy is shown in Fig. 4 as an example.

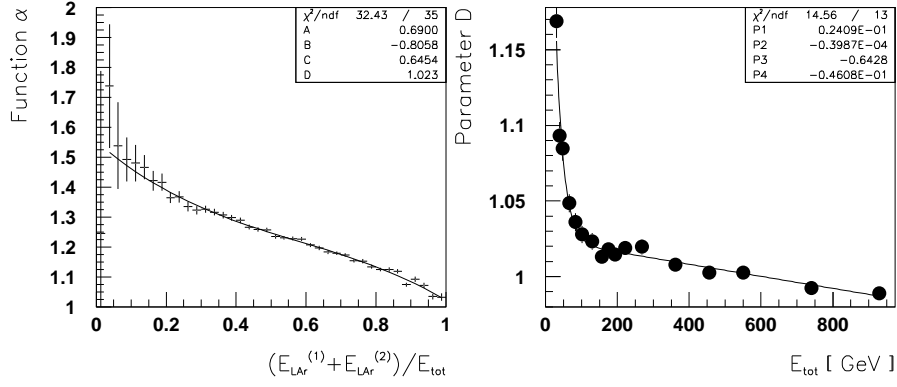


Figure 3: The α function vs. the ratio $(E_{\text{LAr}}^{(1)} + E_{\text{LAr}}^{(2)})/E_{\text{tot}}$ for the 150 GeV gluon jets (left plot). The dependence is fitted according to the formula (12a). The right plot displays the parameter D as a function of the energy E_{tot} . The sum of two exponentials fits this dependence.

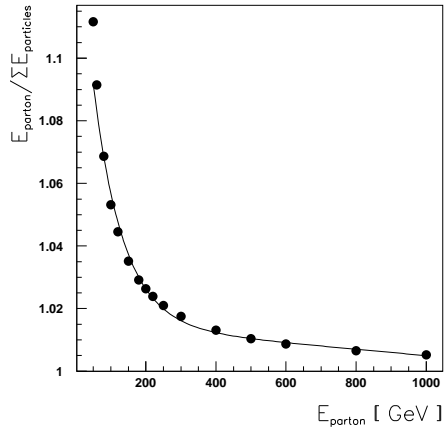


Figure 4: The function β vs. the original gluon energy at the fixed cone size $R = 0.4$. The dependence is described as a sum of two exponentials.

3.2 Results

The parametrization of the α and β functions introduced in the previous section allows us to reconstruct the parton’s original energy. The application of the above described procedure results in a very good linearity ($\pm 0.5\%$) up to 1 TeV, which is important especially for the E_T^{miss} measurement. The resolution improves as well.

As mentioned in Section 2.4, two different noise cuts were applied in the Tile calorimeter prototype modules. The application of the lower cut ($1.5\sigma_{\text{noise}}$) results in slightly better resolution, which manifests itself for the lower jet energies (see Tab. 1). The linearity is the same with both noise cuts used. If not explicitly stated otherwise, further results presented below are obtained with the favoured lower noise cut.

Energy [GeV]	Energy resolution σ/E [%]	
	cut $1.5\sigma_{\text{noise}}$	cut $3\sigma_{\text{noise}}$
50	10.96 ± 0.09	11.29 ± 0.09
60	9.84 ± 0.08	10.10 ± 0.08
80	8.61 ± 0.06	8.85 ± 0.07
100	7.87 ± 0.06	8.04 ± 0.06
120	7.14 ± 0.06	7.31 ± 0.06
150	6.46 ± 0.05	6.66 ± 0.05

Table 1: The energy resolution for gluon jets with two different noise cuts applied in the Tile calorimeter. The lower noise cut is favoured.

The linearity and energy resolution for the gluon jets are shown in Fig. 5, the “raw data” results (i.e. $E_{\text{LAR}} + E_{\text{Tile}}$) are displayed as well for comparison. Due to the technique of summing signal from several single particle events (see Section 2.4), the noise is not constant but roughly proportional to the number of particles in the jet³. Therefore the noise contribution is subtracted from the obtained resolution (see Fig. 5) in order to compare it with the other results (see below).

The resolution obtained for gluon and u-quark jets (both with and without the noise subtracted) is also compared to the single pion resolution obtained with the e/h approach [6] and benchmark method [1]. The results are summarized in Tab. 2. The above described algorithm for parton energy reconstruction results in better energy resolution than do similar methods applied to single pion events, the level of 3% is achieved for 1 TeV jets.

The obtained results are also compared with the energy resolution of light quarks obtained using the ATLAS Monte Carlo [7] in the similar configuration (see Tab. 3). The resolution of the energy reconstructed according to the

³The total noise in one jet event is a quadratic sum of the noise corresponding to single particle events from the beam test data. The beam test noise depends on the number of cells taken into account and is parametrized following the Ref. [1].

Energy [GeV]	Fractional energy resolution σ/E [%]					
	Single pions		Gluon jets		u-jets	
	e/h approach	Benchmark	With noise	Without noise	With noise	Without noise
50	1.41 ± 0.26	1.04 ± 0.17	10.96 ± 0.09	10.51 ± 0.09	10.41 ± 0.08	10.06 ± 0.08
80	8.99 ± 0.18	8.75 ± 0.16	8.61 ± 0.06	8.35 ± 0.07	8.38 ± 0.07	8.18 ± 0.07
100	8.48 ± 0.16	8.23 ± 0.23	7.87 ± 0.06	7.68 ± 0.06	7.73 ± 0.06	7.59 ± 0.06
150	7.44 ± 0.12	6.69 ± 0.13	6.46 ± 0.05	6.34 ± 0.05	6.43 ± 0.05	6.35 ± 0.05
300	5.90 ± 0.11	5.21 ± 0.09	4.90 ± 0.04	4.86 ± 0.04	4.96 ± 0.04	4.92 ± 0.04
500			4.14 ± 0.04	4.12 ± 0.04	4.15 ± 0.03	4.14 ± 0.04
800			3.45 ± 0.03	3.43 ± 0.03	3.67 ± 0.03	3.66 ± 0.03
1000			3.10 ± 0.03	3.09 ± 0.03	3.61 ± 0.03	3.61 ± 0.03

Table 2: The fractional energy resolution for single pions [2, 6] and gluon and u-jets after the applied parton's energy reconstruction. The algorithm used for jets results in better energy resolution than do similar methods applied to single pion events and the 3% resolution is achieved for very high energy jets.

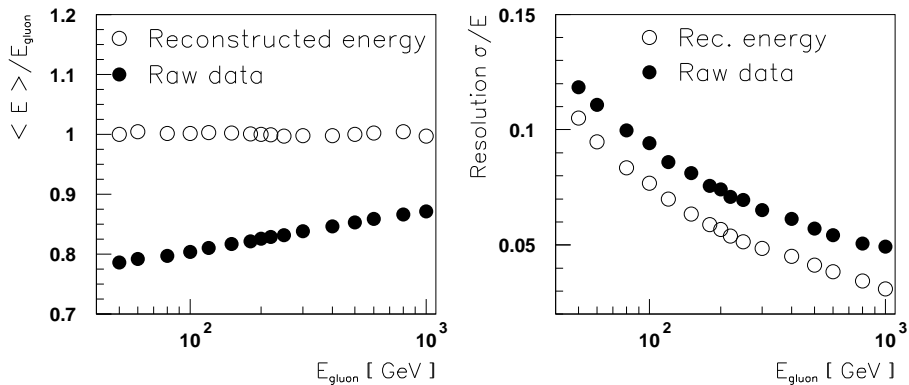


Figure 5: The linearity (left plot) and resolution (right plot) for the gluon jets “raw data” (i.e. $E_{\text{LAR}} + E_{\text{Tile}}$ – full circles) and after the energy reconstruction applied (open circles). The energy reconstruction results in a very good linearity $\pm 0.5\%$ and the resolution improvement. The noise contribution is subtracted in the resolution plot.

formula (6) is worse than that listed in Ref. [7]. Nevertheless, the method presented in the mentioned Ref. recovers only the energy of particles entering the calorimeters (in contrast with the parton energy reconstructed here) and uses 4 energy-dependent weights in the barrel region (presampler, LAr calorimeter, cryostat correction, Tilecal).

Quark Energy [GeV]	Fractional resolution σ/E [%]		
	u-jets		light quarks (MC simulation)
	cut $3\sigma_{\text{noise}}$	cut $1.5\sigma_{\text{noise}}$	
50	10.25 ± 0.09	10.06 ± 0.08	9.3 ± 0.3
200	5.70 ± 0.05	5.68 ± 0.05	4.9 ± 0.2
1000	3.61 ± 0.03	3.61 ± 0.03	2.7 ± 0.1

Table 3: The energy resolution obtained with the presented reconstruction procedure with 2 different noise cuts in the Tilecal prototypes. The u-jets values are listed with subtracted noise (according to the noise parametrization described in Ref. [1]). The results are compared with the ATLAS MC results obtained for the same cone size $R = 0.4$ at $|\eta| = 0.3$ without the noise contribution [7].

Although the parametrization of the α and β functions for u-jets and d-jets coincides, it differs from that obtained for gluon jets. The share of gluon jets with respect to light quark jets decreases with energy, the gluon jet production dominates over the light quarks in the region $|\eta| < 1.6$ up to roughly 400–500 GeV. This favours the gluon parametrization. The u-quark jet linearity

and resolution with the u-quark and gluon jet parametrizations are shown in Fig. 6. Whereas the resolution is almost the same with both parametrizations, the u-quark linearity gets worse with the gluon parametrization. This feature is the same for d,s quarks as well, it is obviously caused by the differences in β functions, whereas the α functions of different partons are very similar.

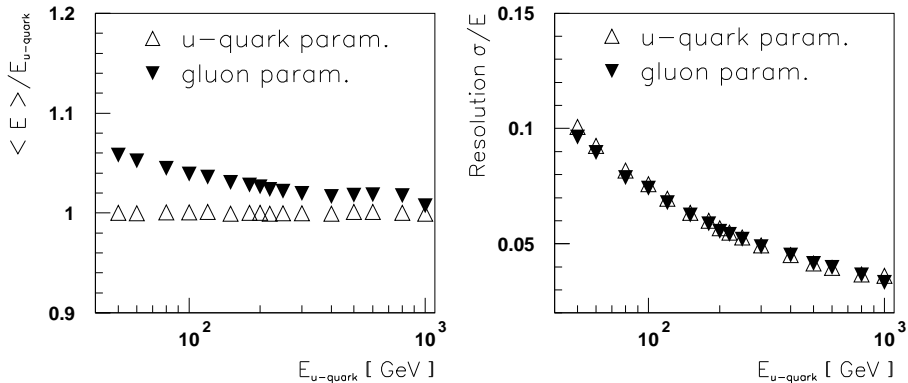


Figure 6: The linearity (left plot) and energy resolution (right plot) for u-quark jets after the energy reconstruction using the “native” u-quark (open triangles) and gluon parameters (full triangles). The noise contribution is subtracted in the resolution plot.

On the other hand, the linearity for heavy quarks c,b is better with the gluon parametrization (compared with that of u-quark). Nevertheless, these energy distributions suffer from large non-Gaussian tails on the lower-energy side due to escaping neutrinos. In c-jets, neutrinos take off in average 3.5% of the primary quark energy (*rms* being 12%), whereas they possess even 7% of the primary quark energy in b-jets with the same spread *rms* = 12%.

4 Energy Reconstruction in LVL1 Trigger

In the LVL1 trigger, the input data represent a set of the so-called trigger towers 0.1×0.1 in $\Delta\eta \times \Delta\varphi$ [8]. The trigger towers are separate for electromagnetic and hadronic calorimeters, nevertheless no information from separate radial calorimeter samplings will be available. Therefore, the above described algorithm for the energy reconstruction has to be slightly modified:

$$E_{\text{rec}} = \beta(E, R) \times \left(\alpha \times c_{\text{LAR}} \times S_{\text{LAR}} + \left(\frac{e}{\pi} \right)_{\text{Tile}} \times c_{\text{Tile}} \times S_{\text{Tile}} \right) \quad (13)$$

where $(e/\pi)_{\text{Tile}}$ and the function $\beta(E, R)$ are the same as described in Section 3.1. The function α now reads

$$\alpha = \alpha \left(\frac{E_{\text{LAR}}}{E_{\text{LAR}} + (e/\pi)_{\text{Tile}} \times E_{\text{Tile}}}, E_{\text{LAR}} + \left(\frac{e}{\pi} \right)_{\text{Tile}} \times E_{\text{Tile}} \right) \quad (14)$$

For the $E_{\text{LAR}} + (e/\pi)_{\text{Tile}} \times E_{\text{Tile}}$ fixed, the α function is parametrized according to the formula (12a), but now with

$$x = \frac{E_{\text{LAR}}}{E_{\text{LAR}} + (e/\pi)_{\text{Tile}} \times E_{\text{Tile}}} \quad (15)$$

As a result, the A , B , C , D parameters dependence on the sum $E_{\text{LAR}} + (e/\pi)_{\text{Tile}} \times E_{\text{Tile}}$ is of the same shape (sum of two exponentials), but with different slopes.

4.1 Results for LVL1 Trigger

The energy reconstruction (13) using the energy sums available at the LVL1 trigger still results in the good linearity and energy resolution improvement with respect to “raw data” (see Fig. 7). The resolution is worse than that using the data from separate samplings (see Tab. 4), nevertheless the results are comparable with the resolution for single pions (see also Tab. 2).

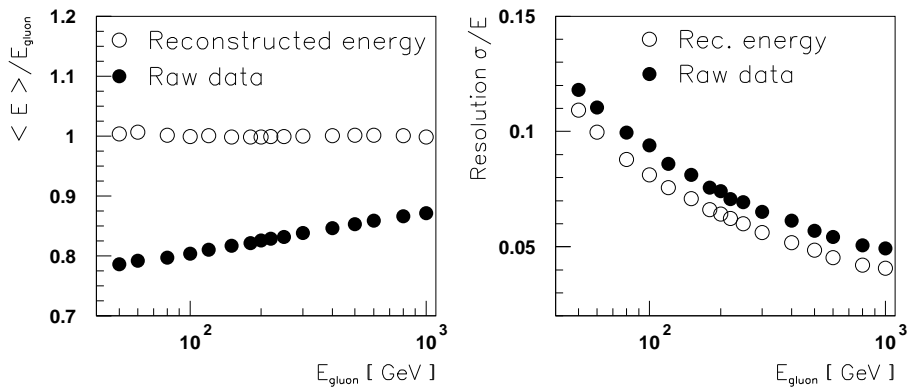


Figure 7: The linearity (left plot) and energy resolution (right plot) for the gluon jets “raw data” (i.e. $E_{\text{LAR}} + E_{\text{Tile}}$ – full circles) and after the energy reconstruction applied according to the formula (13) (open circles). The energy reconstruction results in a very good linearity $\pm 0.5\%$ and the resolution improvement. The noise contribution is subtracted in the resolution plot.

The application of the two different β and α functions (the “native” u-quark and gluon parametrizations) to u-jets gives similar differences as the same procedure in case of the energy reconstruction (6): while the energy resolution is almost the same with both parametrizations, the reconstructed energy with gluon parameters is slightly overestimated, especially for the lower jet energies (see Fig. 8).

Energy [GeV]	Fractional energy resolution σ/E [%]			
	Algorithm (6)		LVL1 trigger (13)	
	gluon jets	u-jets	gluon jets	u-jets
50	10.96 ± 0.09	10.41 ± 0.08	11.41 ± 0.09	10.94 ± 0.08
100	7.87 ± 0.06	7.73 ± 0.06	8.31 ± 0.06	8.48 ± 0.07
300	4.90 ± 0.04	4.96 ± 0.04	5.66 ± 0.04	5.81 ± 0.05
500	4.14 ± 0.04	4.15 ± 0.04	4.87 ± 0.04	5.03 ± 0.04
800	3.45 ± 0.03	3.67 ± 0.03	4.21 ± 0.03	4.57 ± 0.04
1000	3.10 ± 0.03	3.61 ± 0.03	4.08 ± 0.03	4.55 ± 0.04

Table 4: The energy resolution for gluon and u-jets obtained with the algorithm (6) and with its modification for LVL1 trigger (13). All the values are listed without the noise subtraction. The LVL1 trigger results are comparable with the energy resolution of single pions (see also Tab. 2).

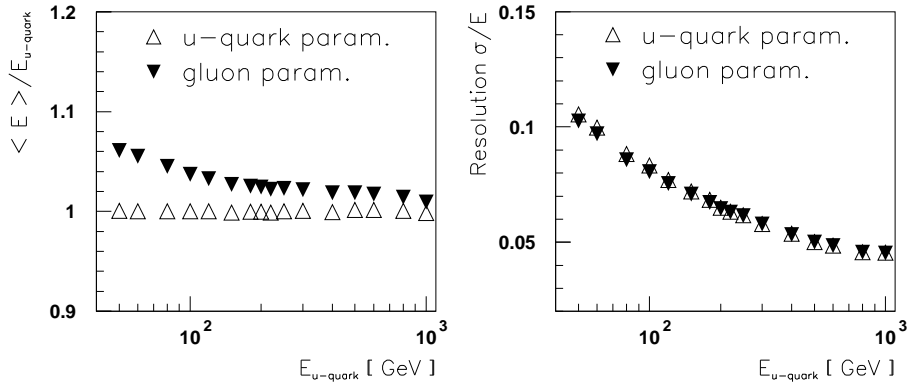


Figure 8: The linearity (left plot) and energy resolution (right plot) for u-quark jets after the energy reconstruction using the “native” u-quark (open triangles) and gluon parameters (full triangles).

5 Conclusion

The method for the reconstruction of the incident parton's energy has been investigated. The presented results were obtained with the calorimeter data from the combined LAr+Tilecal beam test carried out in April 1996.

The applied algorithm results in the very good linearity ($\pm 0.5\%$) and the substantial improvement of the energy resolution with respect to the "raw data". The resolution is even better than that of single pions obtained with similar energy reconstruction techniques [2, 6].

The energy resolution for u-jets is slightly worse than the results obtained with ATLAS MC simulation [7]. The algorithm reported in Ref. [7] reconstructs only the energy of particles entering the ATLAS calorimeter, while the parton energy is recovered in the presented approach.

A simple modification of the above approach for the LVL1 trigger has been studied as well. This algorithm still results in a good linearity (important for the E_T^{miss} measurement) and the energy resolution is comparable with that obtained with similar techniques applied to single pions.

References

- [1] M. Cobal et al: *Analysis Results of the April 1996 Combined Test of the LArgon and Tilecal Barrel Calorimeter Prototypes*, Atlas Note, ATL-TILECAL-98-168, CERN, 1998
- [2] Z. Ajaltouni et al: *Results from an Expanded Combined Test of an Electromagnetic Liquid Argon Calorimeter With a Hadronic Scintillating-Tile Calorimeter*, submitted to NIM A, 1999
- [3] T. Sjöstrand: *Pythia 5.7 and Jetset 7.4*, Comp. Phys. Commun. **28** 227, 1993
- [4] S. Constantinescu, S. Dita: *Separation of Muons, Pions and Protons in Pion Beam*, presentation made on Tilecal analysis meeting, November 1997
- [5] J. Budagov et al: *Electron Response and e/h Ratio of ATLAS Iron-Scintillator Hadron Prototype Calorimeter With Longitudinal Tile Configuration*, Atlas Note, ATL-TILECAL-96-72, CERN, 1996
- [6] Y. A. Kulchitsky et al: *Hadron Energy Reconstruction for the ATLAS Barrel prototype Combined Calorimeter in the Framework of the Non-parametrical Method*, Atlas Note, ATL-TILECAL-2000-005, CERN, 2000
- [7] J. Sjölin: *Jet Reconstruction in the ATLAS Barrel Calorimeter*, Atlas Note, ATL-TILECAL-2000-009
- [8] ATLAS Collaboration: *ATLAS Trigger Performance Status Report*, CERN/LHCC 98-15, CERN, 1998